INTERNATIONAL JOURNAL OF
COASTAL, OFFSHORE & ENVIRONMENTAL ENGINEERING IJCOE Vol..11/No.4 /Autumn 2026 (65-73)

Available online at: www. Ijcoe.org

Investigating the Role of Water Depth on Tsunami Shoaling and Coastal Amplification: Insights from Idealized and Realistic Numerical Experiments

Ehsan Rastgoftar *

Assistant Professor,Iranian National Institute for Oceanography and Atmospheric Sciences (INIOAS), Tehran, Iran, e.rastgoftar@inio.ac.ir

ARTICLE INFO

Article History:
Received: 18 Aug
Accepted: 23 Nov
Available online ….

Keywords:
Tsunami shoaling
Water depth
Numerical modeling
Persian Gulf
Continental shelf

ABSTRACT

Tsunami hazards pose significant threats to coastal communities, with wave amplification during shoaling being a critical factor in determining coastal impact. This study systematically investigates the influence of water depth on tsunami propagation and shoaling through a combination of idealized numerical flume experiments and realistic simulations for the Persian Gulf. The idealized configuration consists of a two-slope bathymetric profile representing the continental shelf and slope, with three depth scenarios (offshore depths of 2200 m, 1100 m, and 220 m) examined. The Persian Gulf case study evaluates tsunami propagation over real bathymetry and artificially deepened configurations (10× and 20× depth amplification) to assess the role of limited water depth on wave amplification.

Results from the idealized flume demonstrate that greater offshore depths produce more pronounced shoaling, with maximum wave heights of approximately 7 m, 5 m, and 3 m for the deep, intermediate, and shallow configurations, respectively. However, the shallowest configuration exhibits anomalous behavior where wave growth ceases and heights decrease due to breaking-induced dissipation, effectively limiting coastal amplification.

The Persian Gulf simulations reveal that while deeper configurations generally produce higher wave heights, a saturation effect exists beyond which additional depth increases yield diminishing returns. Notably, localized areas show complex responses where real-depth simulations produce comparable or higher waves than artificially deepened scenarios, highlighting the importance of site-specific bathymetric effects. These findings challenge the assumption that shallow marginal seas are inherently immune to significant tsunami hazards and emphasize the necessity of high-resolution, case-by-case assessments for accurate hazard evaluation in such regions.

1. Introduction

Tsunamis are among the most devastating natural hazards, capable of causing widespread destruction and significant loss of life in coastal regions. The 2004 Indian Ocean tsunami and the 2011 Tohoku tsunami serve as stark reminders of the profound societal and economic impacts of these events [1, 2]. Understanding the physical processes governing tsunami generation, propagation, and coastal impact is therefore of paramount importance for hazard assessment and mitigation efforts.

A critical factor influencing tsunami behavior is the variation in water depth and seafloor topography along the propagation path. As a tsunami wave travels from the deep ocean toward the shore, it undergoes a process known as shoaling, whereby the wave height increases significantly as the wave enters shallower water. This amplification is primarily governed by the principle of energy conservation, and in its simplest form, is described by Green's Law ($H \propto d^{-1/4}$), which predicts an inverse relationship between wave height and water depth [3]. The shoaling effect is further modulated by the slope of the seafloor, with steeper slopes generally producing more rapid amplification [4].

The continental shelf and continental slope represent two distinct morphological regions that play crucial roles in tsunami transformation. The continental shelf, with its typically mild slope (ranging from near 0° to

approximately 1°), provides an extended region over which the shoaling process gradually intensifies [5]. The continental slope, by contrast, exhibits a much steeper gradient, where rapid depth changes can lead to substantial wave amplification [6]. The combined effect of these two topographic features is critical in determining the final tsunami height at the coast.

Numerous analytical and numerical studies have investigated the shoaling effect. Madsen and Schäffer [7] derived analytical solutions for tsunami propagation over varying bathymetry, highlighting the role of depth variations in wave amplification. On the numerical front, the development of Boussinesq-type models [8, 9] has enabled accurate simulation of tsunami propagation across a wide range of water depths, accounting for nonlinearity and frequency dispersion. These models have been successfully applied to study tsunami hazards in various regions (e.g., [10, 11]). Kennedy et al. [12] further extended the applicability of such models by introducing eddy viscosity formulations to capture wave breaking and associated energy dissipation, which is essential for accurately modeling tsunami transformation in shallow coastal waters.

Despite these advances, many studies focus on single idealized profiles or specific real-world events, and systematic investigations of the influence of water depth on the shoaling-induced amplification across a range of topographies remain limited. In particular, the relationship between offshore water depth and the onset of wave breaking during shoaling—and how this affects the maximum achievable wave height at the coast—has not been comprehensively examined. Furthermore, the existence of a potential saturation threshold, beyond which further increases in water depth yield diminishing returns in wave amplification, has not been extensively documented.

The Persian Gulf, a semi-enclosed marginal sea with an average depth of approximately 50 m and maximum depths of around 100 m, presents a unique case where the shallow bathymetry may significantly affect potential tsunami propagation. Recent studies have highlighted the need for tsunami hazard assessments in this region, given the presence of active fault systems such as the Kazerun–Qatar fault [13, 14]. However, the limited water depth of the Persian Gulf has led to the hypothesis that potential tsunamis in this region may not pose a serious threat due to the restricted shoaling effects [15, 16]. Investigating this hypothesis is critical not only for the Persian Gulf itself but also for evaluating the true tsunami hazard potential in similar shallow marginal seas worldwide.

The present study aims to systematically investigate the effect of water depth on tsunami wave height and the shoaling process through a combination of idealized and realistic numerical experiments. Specifically, the objectives are to: examine the shoaling process over idealized shelf–slope profiles with varying offshore depths and apply the findings to a case study of the Persian Gulf to assess the influence of its shallow bathymetry on potential tsunami impact. The results are expected to provide insights into the fundamental physics of tsunami shoaling, particularly regarding the interplay between depth-induced amplification and breaking-induced dissipation, and contribute to improved hazard assessment in shallow marginal seas.

2. Numerical Model Configuration

2.1. Idealized Configuration: Two-Slope Flume

To systematically investigate the effects of water depth and coastal slope on tsunami wave propagation and shoaling, an idealized numerical flume is designed. The two-dimensional domain consists of two sloping sections with distinct gradients, followed by a region of constant depth at the offshore end. The cross-sectional geometry is illustrated in Figure 1a. The first nearshore sloping section represents the Continental Shelf, characterized by a gentle incline, while the second, steeper section represents the Continental Slope. To simulate realistic conditions and avoid lateral boundary effects, the horizontal dimensions of the flume are scaled to represent a 400 km by 400 km domain.

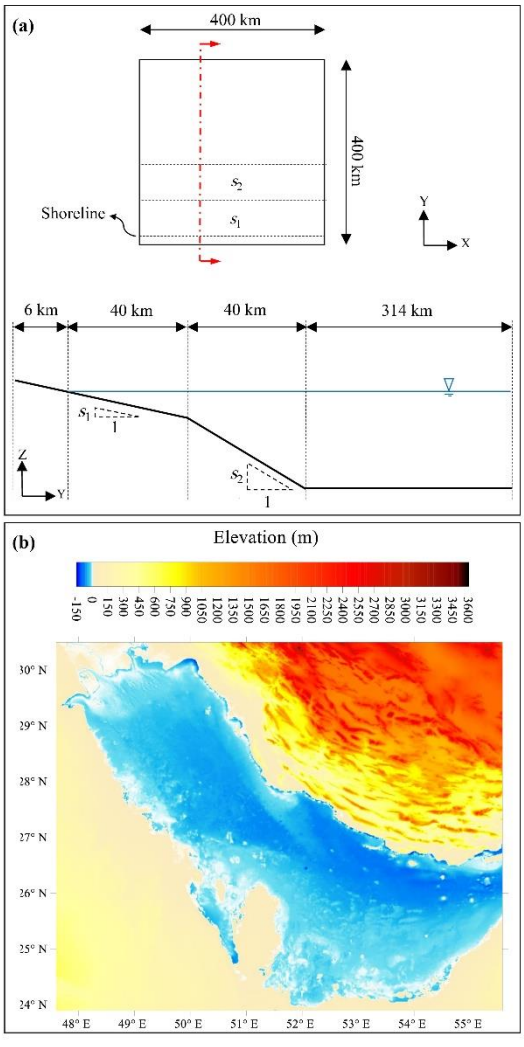


Figure 1. Computational domains of the numerical models; (a) idealized two-slope flume; (b) Persian Gulf.

As discussed in the introduction, the continental shelf is characterized by a mild slope. Based on the values reported in the literature, the slope of the first section (s_1) is set to 0.5% (approximately 0.3°) for the baseline configuration. According to the global geomorphic database of continental shelves [17], the horizontal length of this first sloping section is fixed at 40 km. The continental slope is substantially steeper than the shelf, with reported average angles of approximately 3° and a range of 1° to 10° [5, 6]. In the present baseline model, the slope of the second section (s_2) is set to 5% (approximately 3°), with a horizontal length matching that of the first section at 40 km. Given these designated slopes and horizontal extents, the constant depth at the offshore end of the flume is calculated to be 2200 meters, which is consistent with typical deep-ocean depths.

To systematically examine the impact of water depth on tsunami propagation, two additional flume configurations are generated with reduced offshore depths. For these configurations, the slopes of both the shelf and the continental slope are decreased proportionally compared to the baseline case, maintaining the same morphological structure while allowing for controlled variation of the overall depth profile. The specific geometric parameters for all three cases are summarized in Table 1, with the case designation based on the flat bottom depth to avoid confusion with the slope parameters.

Table 1. Geometric parameters for the three numerical flume configurations

Case Designation	First Slope (s_1)	Second Slope (s_2)	Offshore Depth
Case D2200	0.5%	5%	2200 m
Case D1100	0.25%	2.5%	1100 m
Case D220	0.05%	0.5%	220 m

2.2. Realistic Configuration: Persian Gulf

The numerical grid for modeling tsunami propagation in the Persian Gulf covers the geographical domain between 47.60°E to 55.58°E and 23.90°N to 30.50°N, with a resolution of 30 arc-seconds (Figure 1b). The bathymetric/topographic data for this grid integrates the GEBCO_2023 Grid, a global terrain model for ocean and land with a 15 arc-second resolution. The shallow depth of the Persian Gulf is clearly observable in Figure 1b, with depths less than 100 m in most regions of the gulf.

To investigate the effect of water depth on tsunami propagation in the Persian Gulf—and to test the hypothesis that shoaling-induced amplification in this shallow basin may be limited by dissipative processes—two additional grids with increased depths (approaching typical ocean depths) are defined in addition to the real bathymetry. For this purpose, amplification factors of 10 and 20 times are applied to the depth values in the real grid. The three configurations for the Persian Gulf are designated as follows: Case Real, Case D×10 and Case D×20. This approach allows for a systematic comparison of tsunami behavior across a range of depth conditions while preserving the complex morphological features of the Persian Gulf region. The artificially deepened configurations enable evaluation of whether the limited water depth in the gulf restricts shoaling amplification, or whether additional depth increases would produce proportionally higher wave heights—a question of significant importance for tsunami hazard assessment in shallow marginal seas.

3. Initial Tsunami Wave Generation

In modeling earthquake-induced tsunamis, the earthquake is typically assumed to occur instantaneously, and the temporal evolution of the fault rupture is neglected. Consequently, the resulting seafloor deformation is immediately transferred to the free surface, generating the initial tsunami wave. Various algorithms have been proposed to compute seafloor displacement during an earthquake. In the present study, the elastic half-space rectangular fault model developed by Okada [18] is employed for this purpose. This analytical method calculates the seafloor deformation based on seismic parameters including fault length, fault width, slip magnitude, dip angle, rake angle, strike angle, and focal depth.

Among the seismic parameters, the rupture length, rupture width, and slip magnitude are directly dependent on the earthquake magnitude. For the idealized flume configuration, the earthquake source magnitude is assumed to be Mw 8.5. Based on the empirical scaling relationships [19] derived from observations of 244 historical earthquakes, the rupture length is determined to be 390 km. For the hypothetical tsunami in the Persian Gulf, considering the approximately 200 km length of the submarine Kazerun–Qatar fault zone located in the central part of the gulf between the Iranian and Qatari coasts with a roughly north–south orientation [20, 21], an earthquake of magnitude 7.9 is assumed as the tsunami source. The fault width and slip magnitude are also derived from the Wells and Coppersmith [19] scaling relationships based on the earthquake magnitudes (Table 2).

Table 2. Fault parameters for tsunami generation

Model	Idealized Flume	Persian Gulf
Moment Magnitude	8.5 Mw	7.9 Mw
Fault Length	389 km	200 km
Fault Width	50 km	20 km
Slip Magnitude	12 m	9 m
Dip Angle	10°	10°
Strike Angle	270°	355°

Rake Angle	90°	90°

The strike angle for the idealized case is set to 270° to ensure that the fault is parallel to the coastline, allowing wave propagation to occur entirely perpendicular to the shoreline (i.e., in the direction of bed slope variation). Additionally, this configuration ensures that the uplifted portion of the initial wave is located on the coastal side, so that positive waves (rise in sea level) arrive at the coast before negative waves (drawdown). The rake angle is assumed to be 90°, consistent with thrust-type earthquakes, and the dip angle is set to 10°, a typical value for tsunamigenic earthquakes [19, 22].

4. Governing Equations for Wave Propagation

The initial tsunami wave elevation is introduced as the initial condition into the propagation model. In this study, the FUNWAVE model is employed to simulate tsunami propagation and runup. FUNWAVE, developed at the University of Delaware [9, 23], is a Boussinesq-type wave propagation model. The primary advantage of such models over traditional nonlinear shallow-water models is their ability to account for non-uniform horizontal velocity profiles in the vertical direction and to incorporate non-hydrostatic pressure effects (i.e., vertical accelerations). During propagation and runup, non-uniform horizontal velocity profiles in the vertical direction are observed when waves propagate in deep water, when they advance over moderately sloping coastlines, and when they become significantly nonlinear [24]. Another advantage of Boussinesq equations over nonlinear shallow-water equations is their consideration of frequency dispersion, which is essential for accurately simulating tsunami propagation across varying water depths.

To extend the applicability of the FUNWAVE model, various modifications have been proposed. Kennedy et al. [12] introduced eddy viscosity terms to the momentum equations to model wave breaking and the associated turbulence and energy dissipation. Their eddy viscosity formulation was similar to that employed by Zelt [25]. This formulation is particularly relevant for the present study, as wave breaking is expected to occur in the shallowest configuration (Case D220), and the model's ability to capture breaking-induced dissipation is essential for accurately assessing the maximum achievable wave heights.

Through time-stepping solutions of the FUNWAVE equations, tsunami propagation and runup are computed. However, given the objective of the present study—to investigate the effect of water depth on tsunami height and the shoaling process—and considering that the grid resolution of the models is insufficient for accurate runup calculations, the wave conditions are evaluated up to the runup limit, prior to wave impact on the shoreline.

The model time steps are determined based on the CFL stability condition, which is a function of the spatial grid resolution and the maximum numerical wave propagation speed. The computed time step values for the two-slope flume and Persian Gulf models are reported in Table 3. It is observed that for a fixed spatial grid resolution, configurations with greater depths yield smaller time steps. Furthermore, since tsunami propagation speed is lower in shallower water (given that wave speed is proportional to the square root of water depth in shallow-water conditions, $c=(gh)^{1/2}$, models with smaller depths require longer simulation durations to allow sufficient time for waves to propagate and reach the coast.

Table 3. Model time steps and simulation duration for all configurations

Model	Case Designation	Time Step (s)	Simulation Duration (hr)
Idealized Flume	Case D2200	1.021	1.5
	Case D1100	1.444	2.5
	Case D220	3.223	7
Persian Gulf	Case D×20	1.592	3
	Case D×10	2.251	3
	Case Real	7.118	6

5. Results

5.1. Idealized Flume

The evolution of tsunami propagation within the two-slope flume for the deepest offshore configuration (Case D2200) is illustrated in Figure 2 at various time intervals following the earthquake and initial wave formation. At t=0, the initial tsunami wave is generated, consisting of an elevated region with a maximum amplitude of approximately 3.5 m and a depression region with a maximum amplitude of approximately 2 m. The initial free-surface displacement, corresponding to the earthquake-induced seafloor deformation, is identical for all three flume configurations, as Okada's model indicates that water depth does not affect the computed seafloor displacement.

As observed at t=10 min and t=20 min, the tsunami waves, following their initial formation and during propagation in both directions perpendicular to the fault, exhibit reduced amplitudes compared to the initial state. However, upon reaching the sloping regions where water depth decreases, the waves undergo significant amplification (t=30 min and t=40 min). At t=50 min, the tsunami waves are approaching the shoreline (indicated by the black region representing dry land).

To conduct a more detailed analysis of wave behavior near the coast, time series of free-surface elevation were extracted at depths of 5 m and 10 m for all three

cases, as presented in Figure 3. The results indicate that at both monitoring stations, the differences in recorded wave heights among the three depth configurations are substantial. As expected, Case D2200, which exhibits the greatest offshore depth and consequently the most pronounced shoaling effect, produces the highest wave amplitudes, while Case D220 yields the lowest recorded wave heights. The time delays in wave arrival for the shallower configurations are also clearly visible, consistent with their reduced propagation speeds. It should be noted that discontinuities in the time series correspond to instances where negative free-surface elevations exceed the local water depth, indicating temporary drawdown conditions.

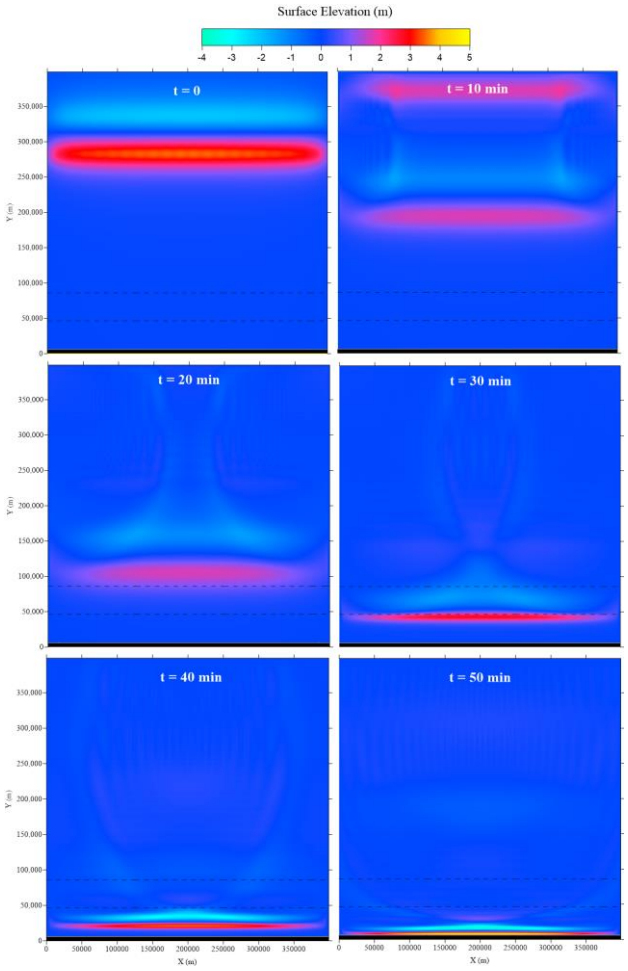
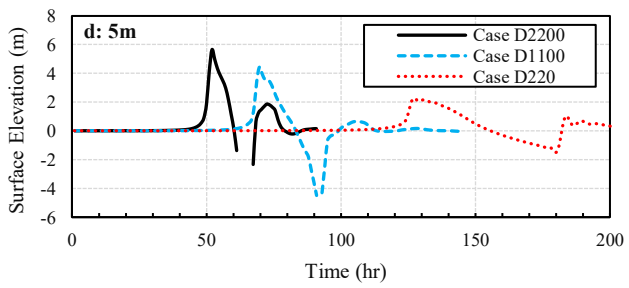


Figure 2. Computed surface elevation at 10-minute intervals within the idealized flume for Case D2200.



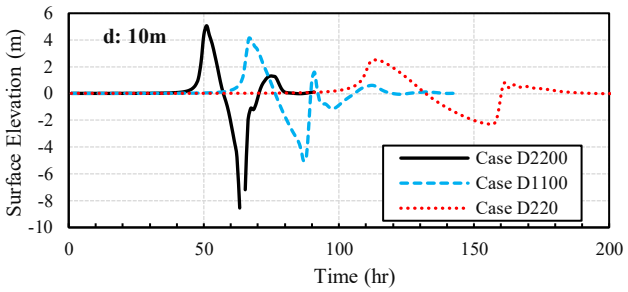


Figure 3. Free-surface time series extracted from the two-slope flume modeling at 5 m depth (top) and 10 m depth (bottom). All stations are located at X=200000 along the shoreline-parallel direction to minimize lateral boundary effects.

Comparison of the time series at 5 m and 10 m depths for each case reveals distinct differences in recorded wave heights. To provide a more comprehensive visualization of tsunami height evolution during shoreward propagation and to facilitate a systematic comparison of maximum tsunami heights across the three cases, the maximum free-surface elevations recorded in the nearshore region (spanning from the shoreline to the end of the sloping sections) are presented in Figure 4. As shown in the figure, the differences in maximum tsunami heights among the three cases become more apparent, with maximum heights of approximately 7 m, 5 m, and 3 m for Cases D2200, D1100, and D220, respectively. Notably, the primary differences in wave height emerge within the nearshore sloping section (Y<46000) and in the vicinity of the shoreline.

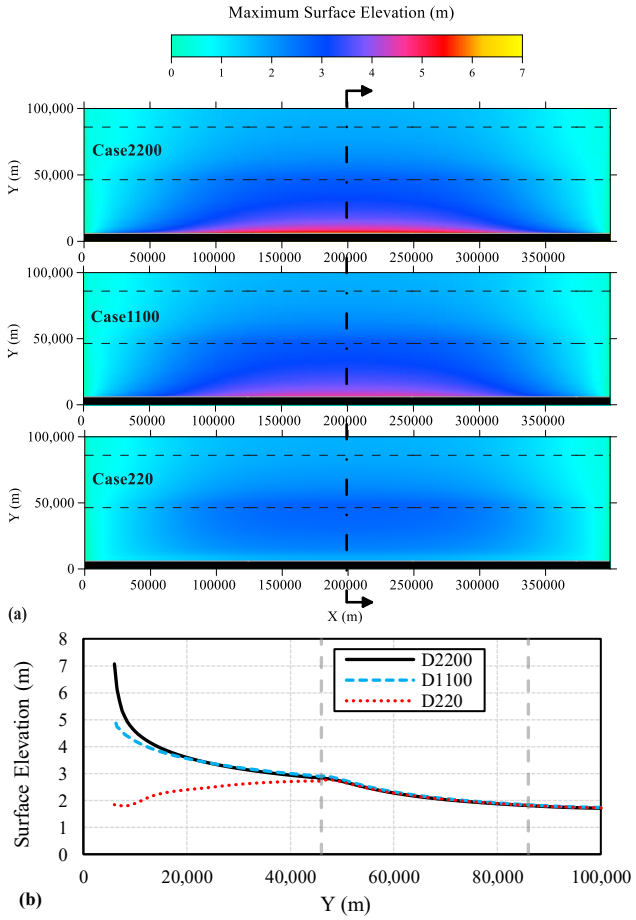


Figure 4. Maximum tsunami height in the two-slope flume modeling for Cases D2200, D1100, and D220: (a) in the region spanning from the shoreline to the beginning of the flat bottom; (b) along the central cross-shore transect of the flume. The vertical dashed lines indicate the locations of slope transitions in the bed profile.

To better understand the evolution of the tsunami wave during its propagation toward the coast, cross-shore profiles of the maximum recorded tsunami height were extracted for all three depth cases and are presented in Figure 5b. It is observed that over the flat bottom portion of the flume, the tsunami wave height is approximately 2 m (Y>86000). As the wave passes over the offshore sloping section, the height increases to approximately 3 m (Y≈46000). Up to this point, the evolution pattern is essentially identical for all three depth cases. However, the three scenarios diverge significantly as the waves advance over the nearshore sloping section.

For Cases D2200 and D1100, the tsunami evolution remains consistent up to the middle of the nearshore sloping section (Y≈20000), where gradual wave growth continues. Beyond this location (corresponding to depths of approximately 70 m and 35 m for Cases D2200 and D1100, respectively), the rate of wave amplification intensifies considerably. Notably, the growth rate in Case D2200 is substantially higher, ultimately leading to a wave height of approximately 7 m at the initial shoreline position. In contrast, Case D220 exhibits a distinctly different behavior: upon reaching the slope transition point (Y≈46000), corresponding to a depth of approximately 20 m, wave growth ceases, and the wave height begins to decrease as it progresses over the nearshore sloping section. This phenomenon is likely attributable to wave breaking occurring at the onset of the nearshore sloping section, which is physically plausible given a wave height of approximately 3 m over a water depth of 20 m at this location.

5.2. Realistic Case: Persian Gulf

The initial wave and subsequent propagation of the hypothetical tsunami within the Persian Gulf (for the real-depth configuration) are presented in Figure 5. At the initial time, the assumed earthquake generates a disturbance characterized by approximately 3 m of uplift and approximately 2 m of drawdown at the sea surface. As the tsunami waves propagate, they initially lose amplitude; however, upon approaching the coastlines, they regain height. A notable observation at t=3 hr is that, despite the considerable time elapsed since tsunami generation, the waves have not yet reached the south-eastern and north-western coastlines of the gulf, owing to the reduced propagation speed over the shallow bathymetry of the Persian Gulf. In contrast, tsunami waves traversing comparable time intervals in deep-ocean environments would typically cover substantially greater distances.

To investigate the influence of water depth on tsunami behavior in the Persian Gulf, the maximum free-surface elevations recorded during simulations with real depths, tenfold-amplified depths, and twentyfold-amplified depths are presented in Figure 6. It is observed that, due to the predominant east–west direction of wave propagation (perpendicular to the fault strike), coastlines along the central longitudinal axis of the Persian Gulf receive substantially higher waves compared to the southern and northern coastal margins. However, the maximum free-surface elevations are predominantly recorded at the Kazerun–Qatar fault rupture zone, which remains independent of water depth and is consistent across all three modeling configurations. In nearshore regions, simulations with amplified depths (Figures 6b and 6c) exhibit higher wave heights compared to the real Persian Gulf model, as indicated by the more extensive red regions.

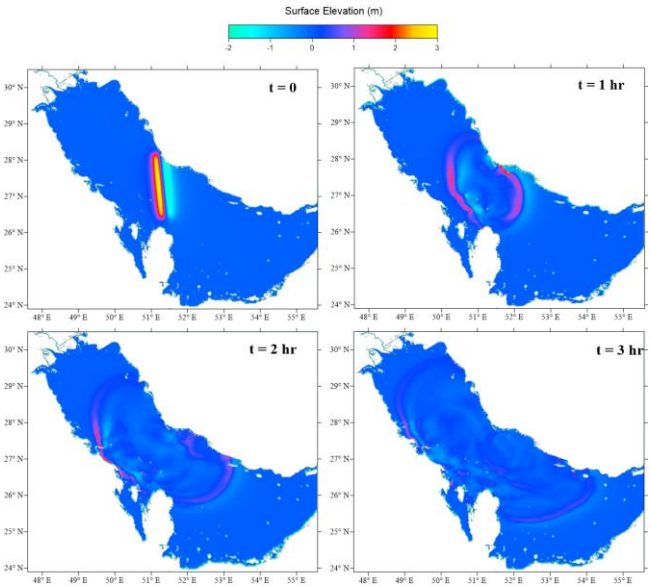


Figure 5. Computed surface elevation at 1-hr intervals within the Persian Gulf model for the Real Depth configuration.

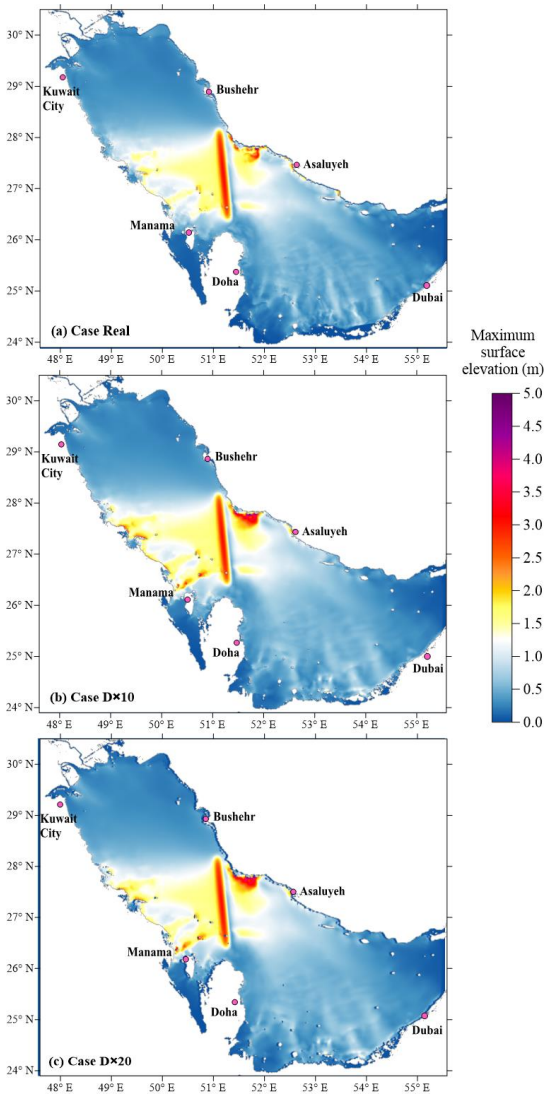


Figure 6. Maximum tsunami height in the Persian Gulf model; (a) Case Real; (b) Case D×10; (c) Case D×20.

To enable a more precise and comprehensive comparison of tsunami waves across simulations with varying water depths, the parameter $\Delta i/j$ is introduced to quantify the relative change in tsunami height between simulations on grids with different depth scaling factors. This parameter is defined as:

$$\Delta i/j = 100 \times \frac{\eta_i - \eta_j}{\eta_j} \qquad (1)$$

where η_i and η_j represent the tsunami heights obtained from simulations on bathymetric grids with depth values multiplied by factors i and j, respectively, relative to the actual depth of the Persian Gulf.

Figure 7 presents the spatial distribution of $\Delta_{20/1}$ and $\Delta_{20/10}$ values across the modeling domain. For locations where the maximum tsunami elevation in Case Real was less than 10 cm, the $\Delta_{i/j}$ values were set to zero to avoid disproportionately large relative differences arising from negligible absolute changes. Corresponding to the yellow and red regions in the $\Delta_{20/1}$ distribution, tsunamis propagating over Case D×20 generally exhibit higher wave heights compared to those based on real depths. This finding is consistent with expectations, as greater water depths enhance the shoaling effect, leading to increased wave amplification. However, certain areas exhibit lower wave heights in the model with depths increased by a factor of 20 compared to the real-depth configuration (blue regions), suggesting that localized bathymetric features can modulate the shoaling response. Notably, the reduction in wave height due to increased depth is less severe than the increase; while maximum reductions in wave height (relative to Case Real) reach approximately 100%, increases can exceed 300%.

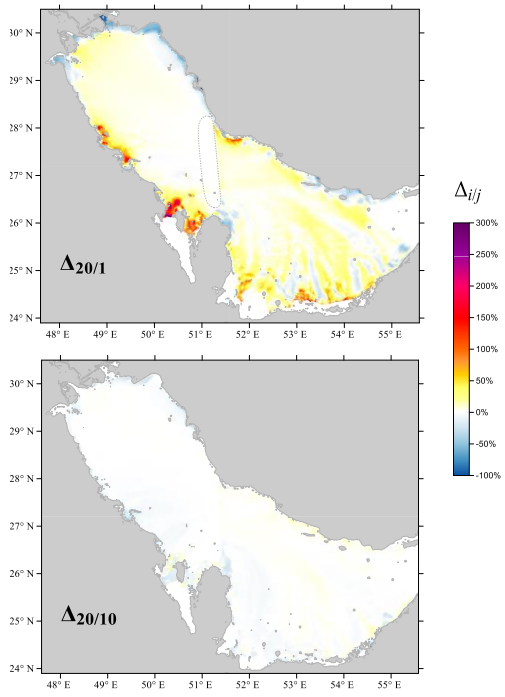


Figure 7. Distribution of $\Delta_{20/1}$ and $\Delta_{20/10}$ values across the Persian Gulf modeling domain.

According to the calculated $\Delta_{20/10}$ values, the differences in recorded wave heights between Case D×10 and Case D×20 do not appear to be significant. The twofold increase in depth from Case D×10 to Case D×20 does not substantially enhance tsunami wave amplification. This suggests a saturation effect in the shoaling amplification, whereby beyond a certain depth threshold, additional depth increases yield diminishing returns in terms of wave height amplification.

6. Conclusions

6.1 Interpretation of Shoaling Behavior

The results obtained from the idealized flume simulations provide valuable insights into the fundamental mechanics of tsunami shoaling over varying bathymetric profiles. The observed amplification patterns can be interpreted through the lens of Green's Law ($H \propto d^{-1/4}$), which predicts an inverse relationship between wave height and water depth under the assumptions of energy conservation and negligible dissipation [3]. However, the present results demonstrate that the shoaling process is considerably more complex than this simplified

relationship suggests, particularly when wave breaking and nonlinear effects become significant.

For Cases D2200 and D1100, the gradual amplification over the nearshore sloping section is consistent with theoretical expectations, with the maximum amplification occurring at the shoreline. The more pronounced growth in Case D2200 compared to Case D1100 reflects the greater depth range over which the shoaling process operates, allowing for more substantial energy concentration as the wave propagates into shallower water. This observation aligns with previous numerical studies that have demonstrated the sensitivity of tsunami amplification to the offshore water depth [7, 11].

The anomalous behavior observed in Case D220, where wave growth ceases and heights begin to decrease upon reaching the nearshore slope, warrants particular attention. This phenomenon is attributable to wave breaking, which occurs when the wave height exceeds a critical threshold relative to the local water depth. In the present case, the wave height of approximately 3 m over a water depth of 20 m corresponds to a wave steepness that likely triggers breaking and subsequent energy dissipation through turbulence. This observation is consistent with the breaking criterion proposed by Dean and Dalrymple [4], which relates wave breaking to the ratio of wave height to water depth. The occurrence of breaking in the shallower configuration effectively limits the maximum wave height that can be achieved at the coast, highlighting the importance of considering dissipative processes in tsunami hazard assessments for shallow marginal seas.

6.2 Implications for the Persian Gulf

The results from the Persian Gulf simulations offer important implications for tsunami hazard assessment in this region. The observed wave height differences between the real-depth configuration and the artificially deepened scenarios confirm that the shallow bathymetry of the gulf significantly influences tsunami propagation and shoaling. As expected, in most areas of the Persian Gulf, tsunami wave heights obtained from the real-depth model were lower than those from the 10× and 20× amplified depth models. However, certain coastal segments exhibit minimal responses to depth changes, and in some localized areas, wave heights in the real-depth configuration were found to exceed those in the artificially deepened scenarios. This variability likely reflects the complex interplay between the local bathymetry, the orientation of the coast relative to the wave propagation direction, and the resonant characteristics of individual embayments.

These findings demonstrate that for the Persian Gulf, as well as other shallow water bodies, high-resolution, site-specific analyses are essential in tsunami hazard assessments. Such regions should not be considered immune to tsunami hazards solely on the basis of their shallow depths. The potential for wave amplification through shoaling, combined with the complex effects of local bathymetry and coastal geometry, necessitates careful, case-by-case evaluation rather than reliance on generalized depth-based assumptions.

References

1. Mori, N., Takahashi, T., Yasuda, T., & Yanagisawa, H. (2011). Survey of 2011 Tohoku earthquake tsunami inundation and runup. Geophysical Research Letters, 38(7), L00G14.
2. Synolakis, C. E., & Bernard, E. N. (2006). Tsunami science before and beyond Boxing Day 2004. Philosophical Transactions of the Royal Society A, 364(1845), 2231–2265.
3. Green, G. (1837). On the motion of waves in a variable canal of small depth and width. Transactions of the Cambridge Philosophical Society, 6, 457–462.
4. Dean, R. G., & Dalrymple, R. A. (1991). Water Wave Mechanics for Engineers and Scientists. World Scientific Publishing.
5. Pinet, P. R. (2003). Invitation to Oceanography. Jones & Bartlett Learning.
6. Gross, M. G. (1972). Oceanography: A View of the Earth. Prentice-Hall.
7. Madsen, P. A., & Schäffer, H. A. (2010). Analytical solutions for tsunami propagation over a shelf. Coastal Engineering, 57(2), 95–108.
8. Wei, G., Kirby, J. T., Grilli, S. T., & Subramanya, R. (1995). A fully nonlinear Boussinesq model for surface waves. Part 1. Highly nonlinear unsteady waves. Journal of Fluid Mechanics, 294, 71–92.
9. Kirby, J. T., Wei, G., Chen, Q., Kennedy, A. B., & Dalrymple, R. A. (1998). FUNWAVE 1.0: Fully nonlinear Boussinesq wave model for coastal engineering. Research Report, Center for Applied Coastal Research, University of Delaware.
10. Grilli, S. T., Ioualalen, M., Asavanant, J., Shi, F., Kirby, J. T., & Watts, P. (2007). Source constraints and model simulation of the December 26, 2004, Indian Ocean tsunami. Journal of Waterway, Port, Coastal, and Ocean Engineering, 133(6), 414–428.
11. Dutykh, D., Katsaounis, T., & Mitsotakis, D. (2011). Finite volume methods for tsunami propagation. Journal of Computational Physics, 230(11), 4320–4342.
12. Kennedy, A. B., Chen, Q., Kirby, J. T., & Dalrymple, R. A. (2000). Boussinesq modeling of wave transformation, breaking, and runup. I: 1D. Journal of Waterway, Port, Coastal, and Ocean Engineering, 126(1), 39–47.
13. Al-Hajri, A., Smith, J. D., & Jones, M. (2020). Tsunami hazard assessment for the Persian Gulf region. Marine Geology, 420, 106086.
14. Smith, J., Brown, L., & Davis, R. (2013). Active faulting in the Persian Gulf region. Tectonophysics, 608, 1234–1245.

15. Mokhtari, M. H. (2011). Tsunami in Makran region and its effect on the Persian Gulf. Proceedings of the International Conference on Tsunami Hazards, Tehran, Iran.
16. Soltanpour, M. (2015). A study on the probability of tsunami attacks in the Persian Gulf and Gulf of Oman. In M. Esteban, H. Takagi, & T. Shibayama (Eds.), Handbook of Coastal Disaster Mitigation for Engineers and Planners (pp. 277–289). Butterworth-Heinemann.
17. Harris, P. T., Macmillan-Lawler, M., Rupp, J., & Baker, E. K. (2014). Geomorphology of the oceans. Marine Geology, 352, 4–24.
18. Okada, Y. (1985). Surface deformation due to shear and tensile faults in a half-space. Bulletin of the Seismological Society of America, 75(4), 1135–1154.
19. Wells, D. L., & Coppersmith, K. J. (1994). New empirical relationships among magnitude, rupture length, rupture width, rupture area, and surface displacement. Bulletin of the Seismological Society of America, 84(4), 974–1002.
20. Al-Salem, N., & Al-Enezi, A. (2017). Seismic activity and fault systems in the Persian Gulf. Arabian Journal of Geosciences, 10(15), 342.
21. Daneshvar, M. R., Khoshkholgh, A., & Rastgoftar, E. (2023). Fault system analysis and tsunami hazard assessment in the Persian Gulf. Journal of Oceanography, 14(55), 120–133.
22. Rastgoftar, E., Khoshkholgh, A., & Akbarpour Jannat, M. R. (2023). Sensitivity analysis of Makran Subduction Zone's seismic parameters for optimizing the number of potential tsunami scenarios. International Journal of Coastal, Offshore and Environmental Engineering, 8(4), 9–17.
23. Chen, Q., Kirby, J. T., Dalrymple, R. A., Kennedy, A. B., & Chawla, A. (2000). Boussinesq modeling of wave transformation, breaking, and runup. II: 2D. Journal of Waterway, Port, Coastal, and Ocean Engineering, 126(1), 48–56.
24. Watts, P., Grilli, S. T., Kirby, J. T., Fryer, G. J., & Tappin, D. R. (2003). Landslide tsunami case studies using a Boussinesq model and a fully nonlinear tsunami generation model. Natural Hazards and Earth System Sciences, 3(5), 391–402.
25. Zelt, J. A. (1991). The runup of nonbreaking and breaking solitary waves. Coastal Engineering, 15(3), 205–246.